Key role of coupling, delay, and noise in resting brain fluctuations

Gustavo Deco[a,b,1], Viktor Jirsa[c,d], A. R. McIntosh[e], Olaf Sporns[f], and Rolf Kötter[g]

[a]Department of Computational Neuroscience, Institució Catalana de Recerca i Estudis Avancats, [b]Universitat Pompeu Fabra, Roc Boronat, 138, 08018 Barcelona, Spain; [c]Theoretical Neuroscience Group, Unité Mixte de Recherche 6233 Institut des Sciences du Mouvement, Centre Nationale de la Recherche Scientifique, 163 Avenue de Luminy, CP 910, 13288 Marseille Cedex 9, France; [d]Center for Complex Systems and Brain Sciences, Physics Department, Florida Atlantic University, 777 Glades Road, Boca Raton, FL 33431; [e]Rotman Research Institute of Baycrest Center, 3560 Bathurst Street, Toronto, ON, Canada M6A 2E1; [f]Department of Psychological and Brain Sciences, Indiana University, Bloomington, IN 47401; and [g]Departments of Neurophysiology and Neuroinformatics, Donders Institute for Brain, Cognition, and Behaviour, Radboud University Medical Centre, 6500 HB Nijmegen, The Netherlands

Edited by Marcus E. Raichle, Washington University School of Medicine, St. Louis, MO, and approved April 10, 2009 (received for review February 19, 2009)

A growing body of neuroimaging research has documented that, in the absence of an explicit task, the brain shows temporally coherent activity. This so-called ''resting state'' activity or, more explicitly, the default-mode network, has been associated with daydreaming, free association, stream of consciousness, or inner rehearsal in humans, but similar patterns have also been found under anesthesia and in monkeys. Spatiotemporal activity patterns in the default-mode network are both complex and consistent, which raises the question whether they are the expression of an interesting cognitive architecture or the consequence of intrinsic network constraints. In numerical simulation, we studied the dynamics of a simplified cortical network using 38 noise-driven (Wilson–Cowan) oscillators, which in isolation remain just below their oscillatory threshold. Time delay coupling based on lengths and strengths of primate corticocortical pathways leads to the emergence of 2 sets of 40-Hz oscillators. The sets showed synchronization that was anticorrelated at <0.1 Hz across the sets in line with a wide range of recent experimental observations. Systematic variation of conduction velocity, coupling strength, and noise level indicate a high sensitivity of emerging synchrony as well as simulated blood flow blood oxygen level-dependent (BOLD) on the underlying parameter values. Optimal sensitivity was observed around conduction velocities of 1–2 m/s, with very weak coupling between oscillators. An additional finding was that the optimal noise level had a characteristic scale, indicating the presence of stochastic resonance, which allows the network dynamics to respond with high sensitivity to changes in diffuse feedback activity.

Recently, a large number of studies have focused attention on spontaneous brain activity during rest (i.e., not associated with any particular stimulus or behavior) (1–5). At the low-scale level of a single cortical area, optical imaging measurements in anesthetized cat visual cortex (V1) have shown how spontaneous activity is clustered in spatiotemporal patterns of neurons with similar orientation preferences (1). At the large-scale level of multiple cortical areas, fMRI studies show that spontaneous blood oxygen level-dependent (BOLD) signal during rest, is characterized by slow fluctuations (<0.1 Hz) and is topographically organized into anticorrelated distributed cortical networks, which are the same networks that are also typically seen during attentional tasks (6–8). The neurophysiological origin of the BOLD signal fluctuations is still unclear, with some evidence suggesting a link to fluctuations in the neural activity and synchrony (9). Furthermore, It seems that slow BOLD signal fluctuations are correlated with EEG power variations of faster rhythms (10, 11), so that they cannot be confounded with the peak frequency of the hemodynamic response function.

Hence, spontaneous activity during rest is not random, but highly organized into reproducible anticorrelated cortical networks. These spatiotemporal patterns have also been shown recently in anesthetized monkeys, demonstrating that they do not seem to be specific for the human, and they do not reflect a state of consciousness (8). Thus, our hypothesis is that these orderly dynamical resting states manifest the intrinsic characteristics of the underlying brain structure.

To understand the mechanisms from which the slow fluctuating and anticorrelated spatiotemporal patterns during rest emerge is not a trivial problem. In complex dynamical systems like the brain, it is very difficult to predict the resulting collective dynamics of the system, even if the underlying topological structure, the local cortical dynamics, and the cortical–cortical interactions are perfectly known. On the other hand, a systematic analysis of the mechanisms generating the collective dynamics of the resting state will provide us with extremely useful information about the intrinsic functional characteristics of the brain.

Existing models provide some important observations (12, 13). In particular, they demonstrate the important role of the characteristic "small-world" structure of the underlying connectivity matrix between different brain areas in the monkey, using realistic neuroanatomical information on the macaque cortex (CoCoMac, see ref. 14), as well as between regions of human cortex (15). Specifically, in ref. 13, it was proposed that the space–time structure of coupling and time delays in the presence of noise defines a dynamic framework for the emergence of the resting brain fluctuations. The aim of this article is to extend the theoretical analysis of the mechanistic origin of the experimentally observed large-scale slow-fluctuating anticorrelated spatiotemporal patterns of the brain at rest. In particular, we want to study the specific intrinsic dynamical characteristics from which the resting patterns emerge. We will investigate the role of connectivity topology, local dynamics, and delays in corticocortical communication and, in particular, the role of noise. We will show that the resting state dynamics strongly depend on all these factors (see ref. 13). In particular, we will show that the resting state results from a stochastic resonance phenomenon, suggesting that the presence of noise is essential for the expression of the spatiotemporal patterns. We will also show how fast local dynamics in the γ-range (40 Hz) generates the slow 0.1-Hz fluctuations at the global level, establishing a specific link between local neuronal communication and global cortical dynamics.

Results

Brain's Intrinsic Properties. The main aim of our investigation is to establish what particular intrinsic properties of brain networks play an essential role in the generation of the most typical aspects of brain dynamics at rest, namely slow oscillations and the emergence

Author contributions: G.D., V.J., A.R.M., O.S., and R.K. designed research; G.D. performed research; G.D., V.J., A.R.M., O.S., and R.K. contributed new reagents/analytic tools; G.D., V.J., A.R.M., O.S., and R.K. analyzed data; and G.D., V.J., A.R.M., O.S., and R.K. wrote the paper.

The authors declare no conflict of interest.

This article is a PNAS Direct Submission.

Freely available online through the PNAS open access option.

[1]To whom correspondence should be addressed. E-mail: gustavo.deco@upf.edu.

This article contains supporting information online at www.pnas.org/cgi/content/full/0901831106/DCSupplemental.

of anticorrelated subnetworks. In particular, we will consider 3 different intrinsic properties: (*i*) neuroanatomical connectivity structure, (*ii*) delays in the transmission of information between different brain nodes, and (*iii*) role of noisy fluctuations.

All simulations and analyses were performed by using a realistic connectivity matrix of the primate brain based on the CoCoMac neuroinformatics tool (14). Kötter and Wanke (16) proposed a coarse parcellation of cerebral cortex into 38 regions, which deliberately reflected broad and rather uncontroversial divisions so that a rough mapping to the human brain appeared feasible. For subsequent activation studies the regional map comprised in addition 2 subcortical thalamic regions, the pulvinar and anterior thalamic nucleus. Connectivity data from tracer studies collated in CoCoMac were transformed to the regional map by using the ORT procedure as described by Stephan et al. (17).

In addition, the center coordinates of the 38 cortical areas were calculated and their distances obtained from the geometry defined in the AAL cortical surface template of a human hemisphere (18). Assuming a uniform velocity of transmission v, we derived approximate delays. The velocity v is one of the free parameters that we consider in our parameter space study. The second parameter that we consider is the global coupling strength α between connected nodes (See *Methods* and SI for details).

The level of noisy fluctuation was also studied parametrically in the next section. We modeled random fluctuations using uncorrelated Gaussian noise that perturbed the population dynamics of each cortical node. Mathematically, this meant we simulated cortical activity by integrating stochastic differential equations based on a simple Wilson–Cowan model of population activity (see below). The origin of this noise could have different sources (see ref. 19). One realistic assumption might be spiking noise. Spiking fluctuations make a significant contribution, because this noise is a significant factor in a network with a finite (i.e., limited) number of neurons. It is important to note that these statistical fluctuations influence, on each trial, the dynamical characteristics of the outcome and not just its time course.

Collective Neurodynamics. We consider in our simulations a very simple neurodynamic model for each node. We assume that each node's dynamics can be captured by a mean-field-like rate model expressing the coupling between excitatory and inhibitory neurons. In particular, we consider the Wilson–Cowan model, which is tuned such that each independent node, if disconnected, is silent (low-activity regime); but because their working point is very near to a Hopf bifurcation, when coupled, each node starts to oscillate. In particular, we choose a working point such that the oscillation of each node, which arises because of coupling, was in the γ-band-range of 40 Hz (see *Methods* and SI for details).

The reason for this choice is that we would like to keep the single node dynamics as simple as possible (oscillatory dynamics) and to concentrate our study on the emergence of a complex collective brain dynamics because of the intrinsic properties mentioned above. Furthermore, by considering simple 40-Hz fast oscillations at the single-node dynamics, we are able to investigate the link between fast local dynamics and slow global fluctuations (10, 11).

First, we study the appropriate working point for our network, i.e., we study the dependence of the collective dynamics as a function of the global coupling strength α and the delays through the velocity parameter v. In particular, because we are interested in cluster synchronization as a possible mechanism for generating the underlying anticorrelated subnetworks typical of the resting state, we first identified a division of the network in clusters using a modularity algorithm (22) (see *Methods* and SI for details). We found that the network can be subdivided in 2 communities (shown in Fig. 1). We note that these 2 communities are highly similar to the ones found in ref. 12.

To study the collective dynamics, we study the level of cluster synchronization in each community as a function of our free

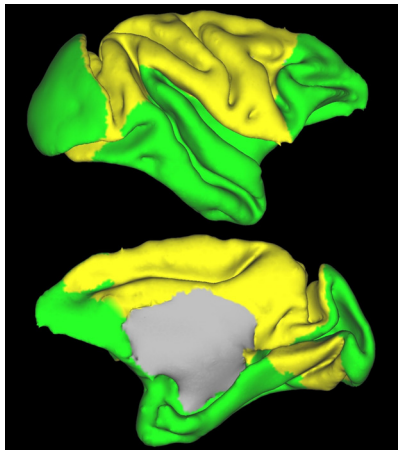

Fig. 1. Anatomical plot of the 2 extracted communities. Shown is a plot of the macaque cortical surface in Caret coordinates (36) with the 2 main clusters indicated in the connection matrix labeled in green and yellow. The green cluster consists mostly of visual areas (with the exception of V2) as well as prefrontal areas. The yellow cluster consists mainly of sensorimotor and premotor areas.

parameters. Two hundred forty seconds of the whole network dynamics were simulated, by employing an optimized Matlab routine (DDESD) based on Runge–Kutta's algorithm. Fig. 2 shows the level of synchronization in each of the 2 extracted communities [i.e., the figure plots the maximum of the Kuramoto indices (defined in *Methods* and SI) of both communities]. The figure shows that for a critical coupling α, there is a transition from a collective silent state (all nodes show low activation) to a synchronized global regime. Nevertheless, the synchronization is relatively low for most of the parameters combinations. However, there are 2 regions of parameter space that show elevated levels of synchronization that correspond to the increase of synchronization in either one of the community clusters: The left bump corresponds to one of the communities and the right bump to the other community. We fix our working point P (indicated Fig. 2 by a black asterisk) between the 2 synchronization bumps ($\alpha = 0.007$ and $v = 1.65$ m/s). The reason is that we expect that in this region, we would find maximal cluster synchronization caused by fluctuations between the synchronization states of the 2 clusters.

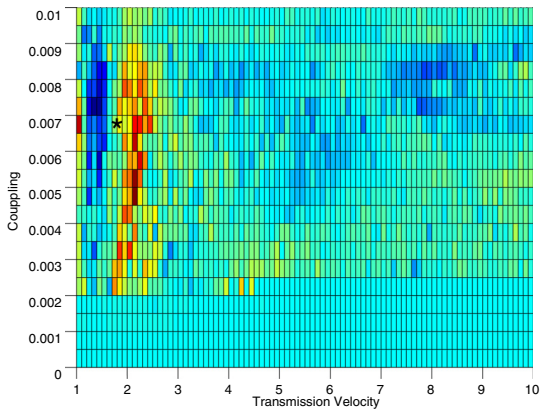

Fig. 2. Parameter analysis of the collective brain network dynamics. The parameters studied are the global coupling α (ordinate) and the delays expressed by the internode communication velocity v (abscissa). The color code is the Kuramoto synchronization index. The black asterisk indicates the chosen working point between the 2 synchronization bumps corresponding to elevated synchronization in one or the other extracted community. The warm colors represent synchronization in the occipital–temporal–prefrontal community, and cold colors represent synchronization in the sensorimotor–premotor community.

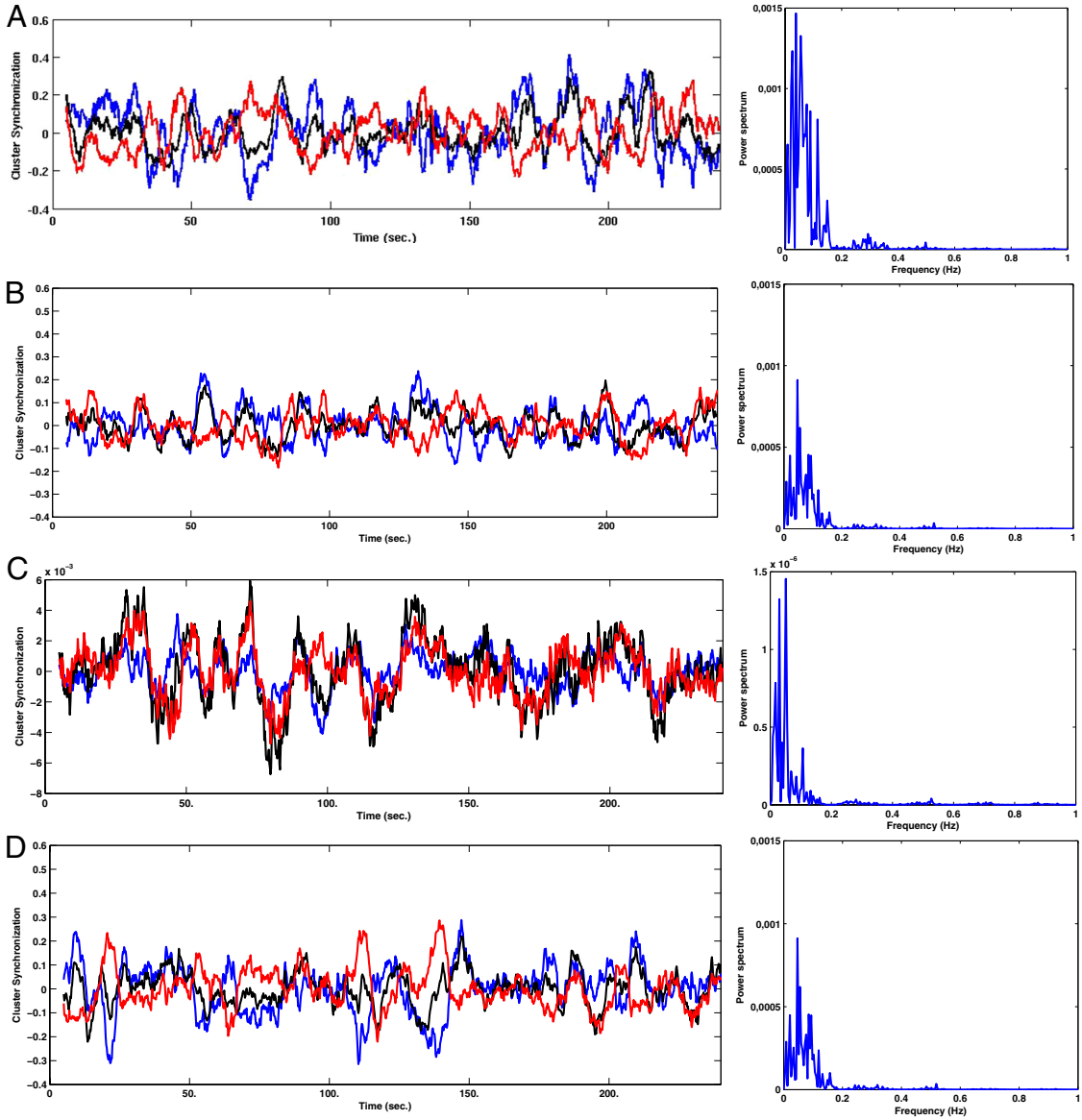

Fig. 3. Synchronization analysis of simulated neuroelectric activity. (*Left*) Level of synchronization for each of the 2 individual communities as measured by the Kuramoto order parameter (community 1, black; community 2, red; difference, blue). (*Right*) Power spectrum of the signal given by differences between the level of synchronization between both communities. (*A*) The results obtained by selecting the optimal working point *P* (see Fig. 2). (*B*) Simulations with a different level of noise ($\langle \nu^2 \rangle = 2$. (*C*) Without delays. (*D*) For a different working point ($\alpha = 0.007$ and $\nu = 3.5$).

Fig. 3*A Left* shows that this working point can reproduce the typical collective brain dynamics found at rest conditions. The black and red curves, respectively, plot the level of synchronization for each of the 2 communities as measured by the Kuramoto order parameter (see *Methods* and SI). The blue curve indicates the differences between the level of synchronization in the 2 clusters. Fig. 3*A Right* shows the power spectrum of the signal given by differences between the level of synchronization between both communities. The figure illustrates that at the chosen optimal working point, both slow 0.1-Hz oscillations of the synchronization signal and anticorrelation of the level of synchronization between the communities occur. However, each community does not show individually a 0.1-Hz modulation of their neural population activity, which underscores the relevance of neural synchronization as a mechanism for the emergence of the ultraslow fluctuations in the BOLD signal. In this figure, the level of noise is optimal ($\langle \nu^2 \rangle = 0.1$), as we will see in the next section. In all these figures, we normalized the results to relative variations with respect to the mean (i.e., $z = (z - \langle z \rangle)/\langle z \rangle$). Note that this normalization is done with respect to the mean of the particular time series of the community under consideration and not with respect to the global brain activity, which may cause artifactual anticorrelation. In other words, the anticorrelation patterns that we find are genuine and not a product of a normalization with respect to the global activity of the whole brain (23).

To study the relevance of the different intrinsic properties of the network we perform the same simulations but with a different level of noise ($\langle \nu^2 \rangle = 2$) (Fig. 3*B*), eliminate the delays (Fig. 3*C*, note the different scaling of the *y* axis), and choose different working points (Fig. 3*D* shows just only 1 case given for $\alpha = 0.007$ and v = 3.5 ms, but similar results were obtained for different working points). These results demonstrate that all these 3 factors are extremely relevant for obtaining the resting-state dynamics. In particular, the velocity parameters are probably constrained by the fact that the relevant emergent resting-state effects result from the equilibrated coordination between the fast local dynamics and the delays in the network. In our case, for the realistic 40-Hz range, we obtained the optimal synchronization level at the above selected working point *P*.

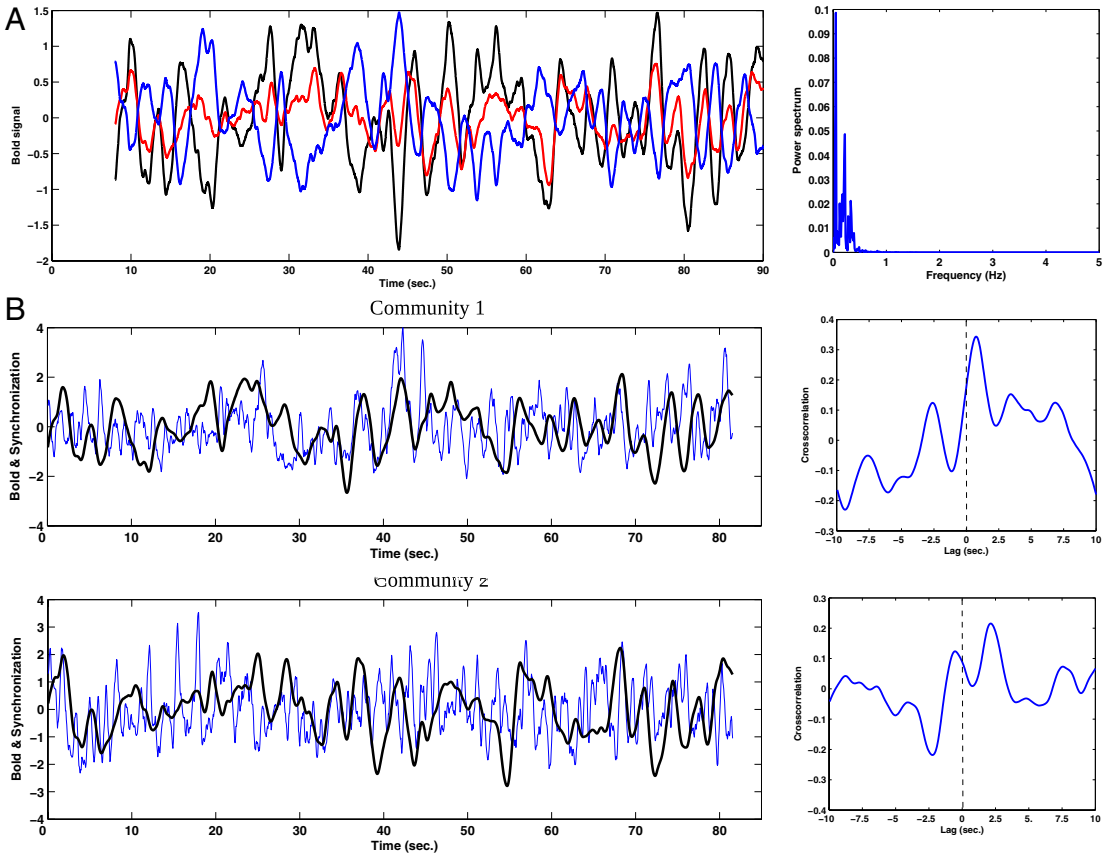

Fig. 4. Sychronization analysis of simulated BOLD data. (*A*) (*Left*) BOLD signal for each of the 2 single communities (community 1, black; community 2, red; difference, blue). (*Right*) Power spectrum of the BOLD signal given by the differences between the level of BOLD signal between both communities. (*B*) (*Left*) Level of synchronization (blue curves) and BOLD signals (black curves) for each of the single communities. The black curves are identical to the black and red curves of *A*. (*Right*) Respective cross-temporal correlations between synchronization and BOLD signals. Note the typical hemodynamics-based delay between 1 and 3 s.

We also calculated the BOLD-signal using the Balloon–Windkessel hemodynamic model of Friston et al. (24), which specifies the coupling of perfusion to the BOLD signal, with a dynamical model of the transduction of neural activity into perfusion changes. Fig. 4*A Left* plots the BOLD signal calculated from the model at the optimal working point *P*. The figure shows that the model can reproduce both the slow 0.1-Hz oscillations and the anticorrelation of the BOLD signals of both communities. The black and red curves plot, respectively, the BOLD signal for each of the 2 single communities. The blue curve represents the difference between the BOLD level in the 2 clusters. Fig. 4*A Right* shows the power spectrum of the BOLD signal given by the differences between the level of BOLD signal in the 2 communities. In all these figures, we normalized the results to relative variations with respect to the mean (i.e., $z = (z - \langle z \rangle / \langle z \rangle)$ (again, note that the normalization is with respect to the mean value of the particular time series, i.e., community under consideration, and not with respect to the whole brain activity). Fig. 4*B* contrasts the relationship between the BOLD signal (black curves) and the level of synchronization (blue curves) on both communities. The curves show that a peak in the Kuramoto synchronization parameter computed from fast voltage–time data reliably precede peaks in the simulated BOLD response. The relationship is offset by a 1- to 3-s hemodynamic delay. Let us note that Honey et al. (12) have also detected a relationship between fluctuations in synchrony and BOLD response, although in the absence of time delays, which is crucial for the mechanism presented here. In conclusion, the 0.1-Hz slow oscillations resulting from alternancy in the level of synchronicity of the 2 communities is the origin of the observed 0.1-Hz slow oscillations of the BOLD signal.

The fact that synchronization predicts BOLD activity is not trivial. This is because the drive to the hemodynamic responses reflects mean population activity and not its synchronization. Our results, therefore, mean that there is a coupling between the degree of synchronization and neural activity that is manifest in elevated BOLD signals. This coupling has been studied in the context of evoked responses (25) and in terms of endogenous fluctuations (26). These analyses of simulated spike trends and local field potentials show that in nearly every domain of parameter space, mean activity and synchronization are tightly coupled, allowing us to conclude that indices of brain activity that are based purely on synaptic activity (e.g., functional magnetic resonance imaging) may also be sensitive to changes in synchronous coupling. Thus, our simulations explain why BOLD might be particularly sensitive to slow fluctuations in fast synchronized dynamics.

Role of Fluctuations: Stochastic Resonance. To study the role and relevance of noise on the collective dynamics of the brain networks, we simulated systematically the behavior of the brain network for different levels of noise. We fixed all parameters according to the optimal working point *P* ($\alpha = 0.007$ and $v = 1.65$ m/s) defined in the previous section and performed the simulations for 240 s. Fig. 5*A* plots the dependence of the maximum of the power spectrum peak of the signal given by differences between the level of synchronization between both communities (measured at the neuronal level as specified above) versus the noise level (variance of the stochastic fluctuations). This gives us a measure of the level of

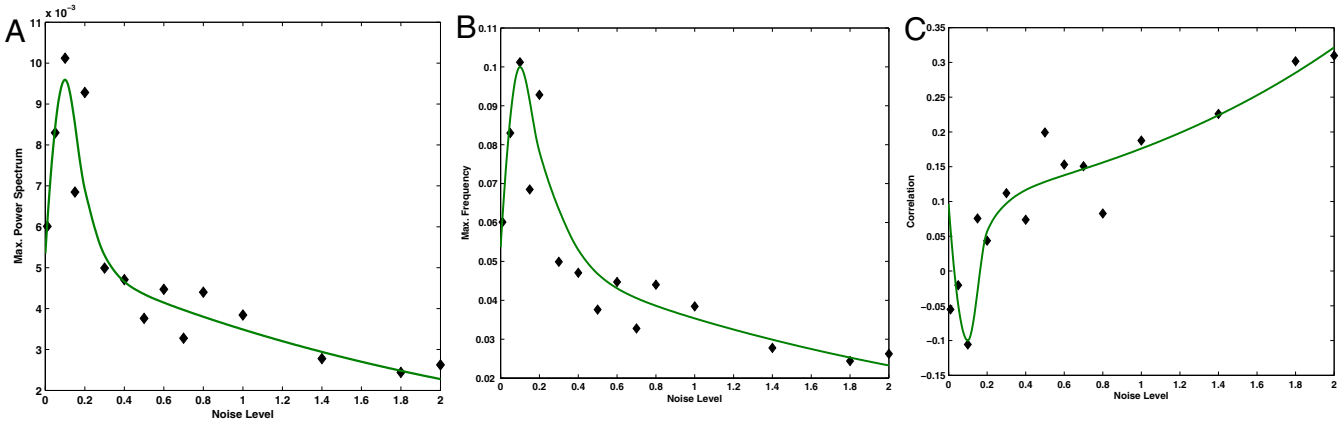

Fig. 5. Stochastic Resonance Effects. (*A*) Maximum of the power spectrum peak of the signal given by differences between the level of synchronization between both communities versus the noise level (variance). (*B*) Maximum in the power spectrum of the signal given by differences between the level of synchronization between both communities versus the noise level. (*C*) Correlation between the level of synchronization between both communities versus the noise level. Note the stochastic resonance effect that for the same level of fluctuations reveals the optimal emergence of 0.1-Hz global slow oscillations and the emergence of anticorrelated spatiotemporal patterns for both communities. Points (diamonds) correspond to numerical simulations, whereas the line corresponds to a nonlinear least-squared fitting using an α-function.

fluctuation that has a maximum effect on the emergence of global oscillations. In all plots, points (diamonds) correspond to numerical simulation results, whereas the lines correspond to a nonlinear least-squared fitting by using an α-function. As the figure shows, there is a stochastic resonance effect, i.e., there is a specified level of noise for which the optimum is reached. Lower or higher levels of noise attenuate the global 0.1-Hz oscillations. Fig. 5*B* plots the dependence of the location (in frequency domain) of the maximum in the power spectrum of the signal given by differences between the level of synchronization between both communities versus the noise level. This measure specifies the position of the maximum of the global oscillation. The figure shows again a stochastic resonance effect for the same level of noise. Furthermore, at this optimal level of noise, the maximum of the spectrum is given by 0.1-Hz global slow oscillations. Finally, Fig. 5*C* plots the level of correlation between the level of synchronization between both communities versus the noise level. Stochastic resonance at the same level of noise reveals a maximum of the anticorrelation between the 2 subnetworks, consistent with the experimental data. It is important to remark that not only the essential role of fluctuations, as documented by the presence of a stochastic resonance effect, but also the fact that the optimum level of fluctuations is given simultaneously for the emergence of 0.1-Hz global slow oscillations and the emergence of anticorrelated spatiotemporal patterns for both communities.

Discussion

In this article, we explored the sensitivity of a simple neural population model of cortical areas with equal intrinsic properties to free parameters in the interareal connectivity model. Although the general connectivity structure was known from a very extensive and systematic collection of anatomical tracer studies in primates (14, 16), it was unclear what dynamics and functional properties would emerge beyond what was known from previous topological studies (13, 27). It turned out that the system of coupled (Wilson–Cowan) oscillators was highly sensitive to systematic variations in propagation velocity and coupling strength. The latter is fully in line with a previous study by ref. 28, where a much simpler static model was updated in arbitrary time steps. Of course, it is also important that the system is at an appropriate working point to display its behavior. We chose both propagation velocity and coupling efficiency such that the system could easily go back and forth between 2 states, where sets of areas synchronized temporarily and formed 2 anticorrelated communities. This was possible on the basis of a subthreshold level of noise that, by itself, would not be sufficient to induce oscillations in individual nodes but only in the connected system. In fact, this level of noise would then drive the coupled oscillators to explore the multistable trajectory of the system.

What we found as the optimal values to put the system into this sensitive state are plausible values implying a conductance velocity of $\approx$1.5 m/s (projected to the size of the human brain), a low coupling strength α of 0.007 (making up for the reduced sparseness of a coarse connectivity matrix), and a noise level that does not induce strong self-sustaining oscillatory states (as seen in epileptic, conditions). These results are fully consistent with the parameter ranges found in (13, 27), where the authors identified emergent resting-state networks characteristic for these regimes. Beyond the parametric study, we obtained insights into the functional organization of the cerebral cortex, using a matrix that comprises an entire hemisphere. Similar to a previous study by ref. 12, we observed 2 synchronized communities of areas, which were anticorrelated. The network of ref. 12, however, comprised only the visual and sensorimotor cortices, albeit at a higher resolution. There, the authors identified similarly a dorsal and a ventral network with 2 connector hubs (area 46, in the present nomenclature: PFCcl; and V4, here part of VACv) that were involved in switching between them. In the present study and in refs. 13 and 27, noise and the time delays via signal propagation were essential to produce this behavior, whereas in the former one by ref. 12, these complex dynamics occurred even in the absence of noise and delays because of the intrinsic nonlinearity and chaotic nature of the mean-field model used.

Although several sources of noise are likely present in the brain (e.g., spontaneous synaptic vesicle release, temperature-dependent Brownian motion of molecules; stochastic opening of ion channels, etc.), it is unlikely that noise is a robust signal that encodes information. Nevertheless, the use of noise to enhance information processing is implied in the current study employing a phenomenon referred to as "stochastic resonance." This phenomenon may help to explain variations in processing within and between individuals, and its mechanism may be related to more specific signals used in so-called "top-down" or "feedback" modulation of signal processing. There is now emerging experimental (29, 30) and computational (31, 32) evidence that those signals do actually play an important role in cognition, and it will be important to explore their more precise role in future more detailed models that implement the different laminar characteristics of interarea projections.

A particular relevant contribution of this article is to show how patterns of anticorrelation emerge in the global dynamics without the use of long-range inhibition (which is generally absent between brain areas). The key idea was to associate the patterns of anticorrelation as reported in the fMRI literature with the level of synchronization between different brain areas. We have shown that the level of synchronization is directly associated with the BOLD-signal. Furthermore, the anticorrelation patterns emerges as the result of noise-driven transitions between different multistable cluster synchronization states (in our case, each pattern corresponding to maximal synchronization on each community). This multistable state appears in coupled oscillators systems because of the delay transmission times underwriting the importance of the space–time structure of couplings in networks (see also ref. 27), where the anatomical connectivity captures the spatial component and the transmission time delays the temporal component thereof. We believe that the particular dynamics of the intrinsic properties of the brain are useful for keeping the system in a high competition state between the different subnetworks that later are used during different tasks. In this way, a relatively small external stimulation is able to stabilize one or the other subnetwork giving rise to the respective evoked activity. So, the anticorrelated fluctuating structure of the subnetwork patterns characteristic of the resting state is particularly convenient for that. Metaphorically speaking, the resting state is like a tennis player waiting for the service of his opponent. The player is not statically at rest, but rather actively moving making small jumps to the left and to the right, because in this way, when the fast ball is coming, he can rapidly react. In this way, an active resting state (fluctuating between multistable states) can be sensitive to external signals that can trigger the activation of one of several available multistable states. This extends to the level of global dynamics a principle that was demonstrated at the level of local dynamics, where the competitive balance between excitation and inhibition ensures the emergence of unified network states that are important for local processing in attention, memory, and decision making (33).

Methods

Connectivity Data on the Macaque Brain. To study the intrinsic properties of the brain at rest, we performed all of the simulations and analyses using a connectivity matrix for 1 macaque hemisphere based on data from the neuroinformatics database CoCoMac (http://cocomac.org).

Network Dynamics. The collective dynamics of a network of identical neuronal populations is determined only by the neuroanatomical connectivity matrix, if the dynamics of the single nodes is simple (e.g., Kuramoto oscillators) and if the transmission of information between different cortical nodes is instantaneous. Honey et al. (12) have shown that a much richer and more complex behavior (like the one evidenced during resting state) could emerge if the single-node dynamics are more complex (in particular, they used a more elaborate neuronal population dynamics that shows chaotic behavior). Another method to get a more complex collective network dynamics is by using a simple dynamics for each node but assuming realistic delay in the signal transmission between nodes in the network.

In this article, we concentrate on this last alternative. We assume realistic delays and take a simple realistic dynamics given by a Wilson–Cowan oscillator (35). The reason for this is that we would like to focus on the role of delays and, at the same time, consider how the typical global slow oscillation at rest could emerge from a network built up with simple fast oscillators (in the γ-band of 40 Hz). The equations describing the dynamics are given in the SI.

Cluster Synchronization. Cluster synchronization is studied by defining a Kuramoto order parameter for each community in a sliding time window of 500 ms shifted by steps of 50 ms. We first shift the excitatory (x) and inhibitory (y) component of all nodes in a value μx and μy, respectively (i.e., $x = x - \mu^x$ and $y = y - \mu^y$), such that the oscillations are centered around the origin. In each time window starting at time t_i and ending at time t_f, a measure of the degree of synchronization in each community M is given by,

$$K'_M(t_f) = \left\langle \left| \sum_{n\in M} x_n(t) - \left\langle \sum_{n\in M} x_n(t) \right\rangle + \hat{\imath}\left(\sum_{n\in M} y_n(t) - \left\langle \sum_{n\in M} y_n(t) \right\rangle \right) \right| \right\rangle \qquad [1]$$

where $\langle\rangle$ denotes average over time along the corresponding time window, and $\hat{\imath}$ is the imaginary unit. In all cases, we plot the normalized Kuramoto parameter normalized over all time windows along, i.e.

$$K_M(t_f) = \frac{K'_M(t_f) - \langle K'_M(t_f)\rangle}{\langle K'_M(t_f)\rangle} \qquad [2]$$

where now the average is taken over all time windows.

1. Arieli A, Sterkin A, Grinvald A, Aertsen A (1996) Dynamics of ongoing activity: Explanation of the large variability in evoked cortical responses. *Science* 273:1868–1871.
2. Biswal B, Yetkin F, Haughton V, Hyde J (1995) Functional connectivity in the motor cortex of resting human brain using echo-planar MRI. *Magn Reson Med* 34:537–541.
3. Shulman G, et al. (1997) Common blood flow changes across visual tasks: II. Decreases in cerebral cortex. *J Cognit Neurosci* 9:648–663.
4. Gusnard D, Raichle M (2001) Searching for a baseline: Functional imaging and the resting human brain. *Nat Rev Neurosci* 2:685–694.
5. Raichle M, Mintun M (2006) Brain work and brain imaging. *Annu Rev Neurosci* 29:449–476.
6. Grecius M, Krasnow B, Reiss A, Menon V (2003) Functional connectivity in the resting brain: A network analysis of the default mode hypothesis. *Proc Natl Acad Sci USA* 100:253–258.
7. Fox M, et al. (2005) The human brain is intrinsically organized into dynamics, anticorrelated functional networks. *Proc Natl Acad Sci USA* 102:9673–9678.
8. Vincent J, et al. (2007) Intrinsic functional architecture in the anaesthetized monkey brain. *Nature* 447:83–86.
9. Nir Y, et al.. (2008) Interhemispheric correlations of slow spontaneous neuronal fluctuations revealed in human sensory cortex. *Nat Neurosci* 11:1100–1108.
10. Mantini D, Perrucci M, Del Gratta C, Romani G, Corbetta M (2007) Electrophysiological signatures of resting state networks in the human brain. *Proc Natl Acad Sci USA* 104:13170–13175.
11. Monto S, Palva S, Voipio J, Palva M (2008) Very slow EEG fluctuations predict the dynamics of stimulus detection and ascillation amplitudes in humans. *J Neurosci* 28(33):8268–8272.
12. Honey C, Kötter R, Breakspear M, Sporns O (2007) Network structure of cerebral cortex shapes functional connectivity on multiple time scales. *Proc Natl Acad Sci USA* 104:10240–10245.
13. Ghosh A, Rho Y, McIntosh A, Kötter R, Jirsa V (2008) Noise during rest enables the exploration of the brain's dynamic repertoire. *PLoS Comput Biol* 4:e1000196.
14. Kötter R (2004) Online retrieval, processing, and visualization of primate connectivity data from the cocomac database. *Neuroinformatics* 2:127–144.
15. Honey C, et al. (2009) Predicting human resting-state functional connectivity from structural connectivity. *Proc Natl Acad Sci USA* 106:2035–2040.
16. Kötter R, Wanke E (2005) Mapping brains without coordinates. *Phil Trans R Soc London Ser B* 360:751–766.
17. Stephan K, Zilles K, Kötter R (2000) Coordinate-independent mapping of structural and functional data by objective relational transformation (ort). *Phil Trans R Soc London Ser B* 355(1393):37–54.
18. Tzourio-Mazoyer N, et al. (2002) Automated anatomical labeling of activations in spm using macroscopic anatomical parcellation of the mni MRI single-subject brain. *NeuroImage* 15:273–289.
19. Faisal A, Selen L, Wolpert D (2008) Noise in the nervous syste. *Nat Rev Neurosci* 9:292–303.
20. Mattia M, Del Giudice P (2004) Finite-size dynamics of inhibitory and excitatory interacting spiking neurons. *Phys Rev E* 70:052903.
21. Mattia M, Del Giudice P (2002) Attention and working memory: A dynamical model of neuronal activity in the prefrontal cortex. *Phys Rev E* 66:51917–51919.
22. Leicht E, Newman M (2008) Community structure in directed networks. *Phys Rev Lett* 100:118703.
23. Murphy K, Birn R, Handwerker D, Jones T, Bandettini P (2009) The impact of global signal regression on resting state correlations: Are anti-correlated networks introduced? *NeuroImage* 44:893–905.
24. Friston K, Harrison L, Penny W (2003) Dynamic causal modelling. *NeuroImage* 19:1273–1302.
25. Chawlam D, Lumer E, Friston K (2000) Relating macroscopic measures of brain activity to fast dynamic neural interactions. *Neural Comput* 12:2805–2821.
26. Chawla D, Lumer E, Friston K (1999) The relationship between synchronisation among neural populations and their mean activity levels. *Neural Comput* 11:1389–1411.
27. Ghosh Y, Rho A, McIntosh R, Kötter R, Jirsa V (2008) Cortical network dynamics with time delays reveals functional connectivity in the resting brain. *Cognit Neurodyn* 2:115–120.
28. Kötter R, Sommer F (2000) Global relationship between anatomical connectivity and activity propagation in the cerebral cortex. *Phil Trans R Soc London Ser B* 355(1393):127–134.
29. Winterer G, et al. (1999) Cortical activation, signal-to-noise ratio and stochastic resonance during information processing in man. *Clin Neurophysiol* 110:1193–1203.
30. McIntosh A, Kovacevic N, Itier R (2008) Increased brain signal variability accompanies lower behavioral variability in development. *PLoS Comput Biol* 4:e1000106.
31. Frank T, Daffertshofer A, Beek P, Haken H (1999) Impacts of noise on a field theoretical model of the human brain. *Physica D* 127:233–249.
32. Kosko B, Mitaim S (2001) Robust stochastic resonance: Signal detection and adaptation in impulsive noise. *Phys Rev E* 64:051110.
33. Brunel N, Wang XJ (2001) Effects of neuromodulation in a cortical network model of object working memory dominated by recurrent inhibition. *J Comput Neurosci* 11:63–85.
34. Stephan K, et al. (2001) Advanced database methodology for the collation of connectivity data on the macaque brain (cocomac). *Phil Trans R Soc London* 356:1159–1186.
35. Wilson H, Cowan J (1972) Excitatory and inhibitory interactions in localised populations of model neurons. *Biophys J* 12:1–24.
36. Van Essen DC, et al. (2001) An integrated software system for surface-based analyses of cerebral cortex. *J Am Med Inform Assoc* 8:443–459.

Corrections

NEUROSCIENCE

Correction for "Key role of coupling, delay, and noise in resting brain fluctuations," by Gustavo Deco, Viktor Jirsa, A. R. McIntosh, Olaf Sporns, and Rolf Kötter, which appeared in issue 25, June 23, 2009, of *Proc Natl Acad Sci USA* (106:10302–10307; first published June 3, 2009; 10.1073/pnas.0901831106).

The authors note that on page 10304, in Fig. 3*D*, the right-hand graph was incorrect as shown. Additionally, on page 10306, Fig. 5*B* was incorrect as shown. These errors do not affect the conclusions of the article. The corrected figures and their legends appear below.

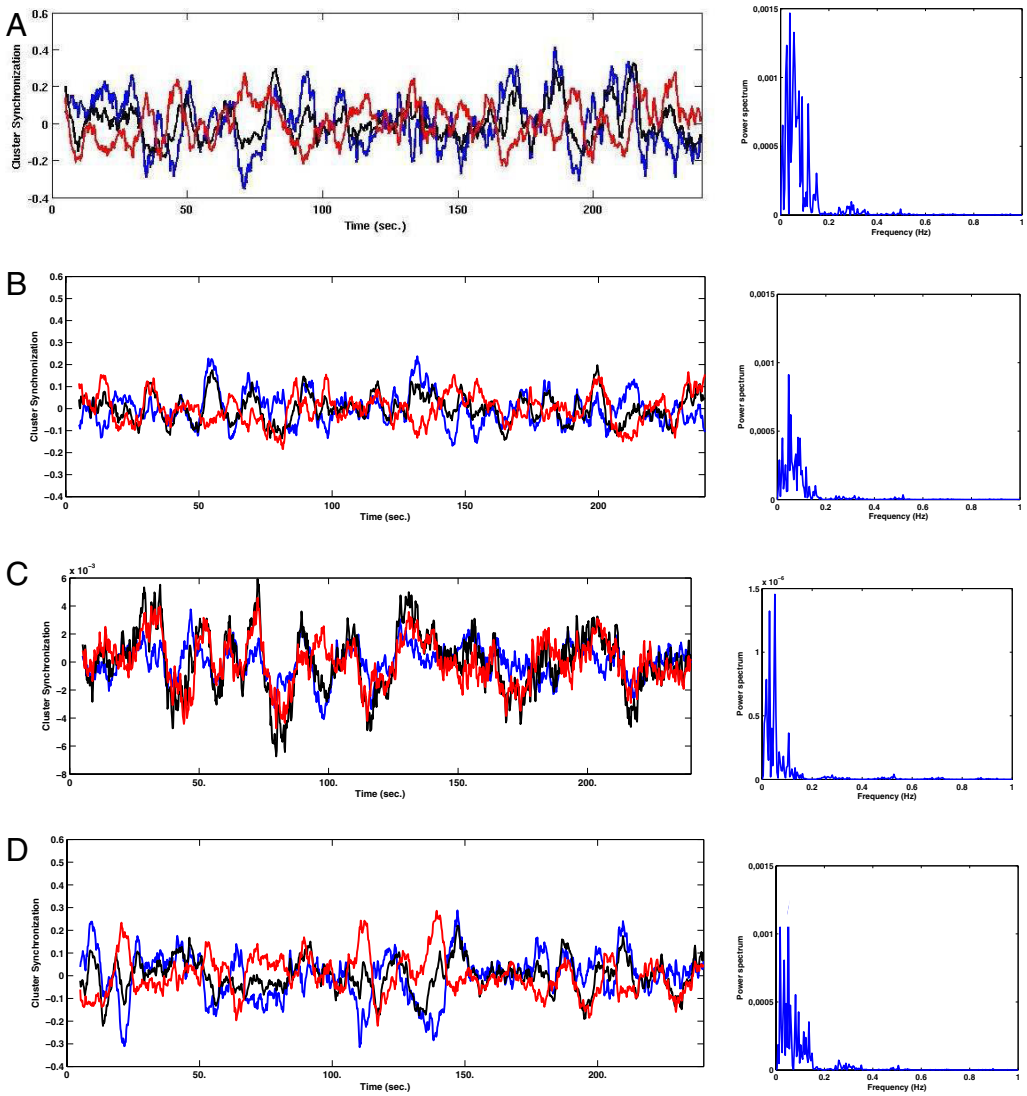

Fig. 3. Sychronization analysis of simulated neuroelectric activity. (*Left*) Level of synchronization for each of the 2 individual communities as measured by the Kuramoto order parameter (community 1, black; community 2, red; difference, blue). (*Right*) Power spectrum of the signal given by differences between the level of synchronization between both communities. (*A*) The results obtained by selecting the optimal working point *P* (see Fig. 2). (*B*) Simulations with a different level of noise ($\langle \nu^2 \rangle = 2$). (*C*) Without delays. (*D*) For a different working point ($\alpha = 0.007$ and $\nu = 3.5$).

CORRECTIONS

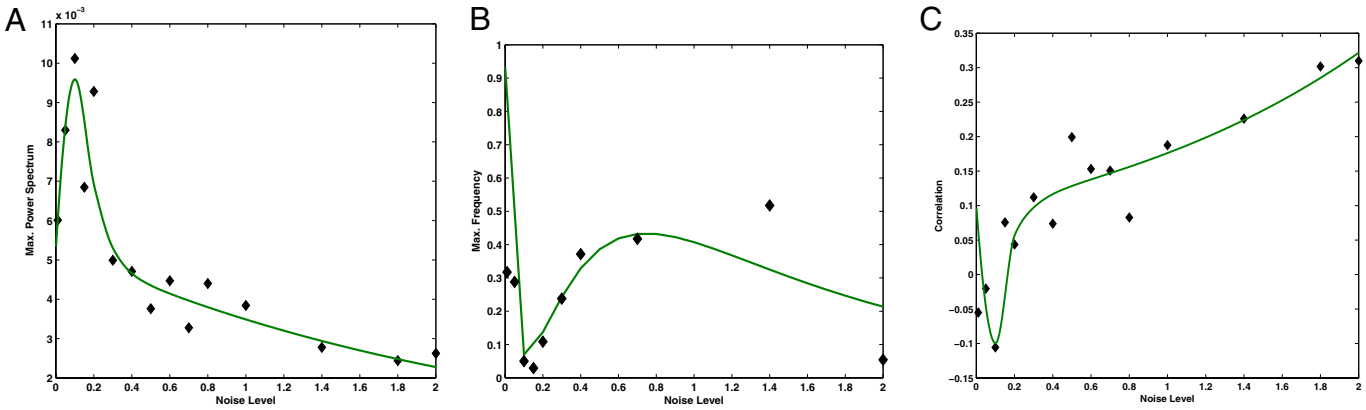

Fig. 5. Stochastic resonance effects. (*A*) Maximum of the power spectrum peak of the signal given by differences between the level of synchronization between both communities versus the noise level (variance). (*B*) Maximum in the power spectrum of the signal given by differences between the level of synchronization between both communities versus the noise level. (*C*) Correlation between the level of synchronization between both communities versus the noise level. Note the stochastic resonance effect that for the same level of fluctuations reveals the optimal emergence of 0.1-Hz global slow oscillations and the emergence of anticorrelated spatiotemporal patterns for both communities. Points (diamonds) correspond to numerical simulations, whereas the line corresponds to a nonlinear least-squared fitting using an α-function.

www.pnas.org/cgi/doi/10.1073/pnas.0906701106

NEUROSCIENCE

Correction for "Extensive remyelination of the CNS leads to functional recovery," by I. D. Duncan, A. Brower, Y. Kondo, J. F. Curlee, Jr., and R. D. Schultz, which appeared in issue 16, April 21, 2009, of *Proc Natl Acad Sci USA* (106:6832–6836; first published April 2, 2009; 10.1073/pnas.0812500106).

The authors note that on page 6836, right column, first paragraph, the fourth line appears incorrectly in part. The dose amount "25.0 and 50.0 Gy" should instead appear as "25–50 kGy." This error does not affect the conclusions of the article.

www.pnas.org/cgi/doi/10.1073/pnas.0906582106

BIOPHYSICS AND COMPUTATIONAL BIOLOGY

Correction for "Dissection of the high rate constant for the binding of a ribotoxin to the ribosome," by Sanbo Qin and Huan-Xiang Zhou, which appeared in issue 17, April 28, 2009, of *Proc Natl Acad Sci USA* (106:6974–6979; first published April 3, 2009; 10.1073/pnas.0900291106).

The authors note that García-Mayoral et al. (42) also studied the interaction between loop 1 of the ribotoxin and ribosomal protein L14 by docking their structures together. The present paper focuses on the binding kinetics. The reference citation appears below.

42. García-Mayoral F, et al. (2005) Modeling the highly specific ribotoxin recognition of ribosomes. *FEBS Lett* 579:6859–6864.

www.pnas.org/cgi/doi/10.1073/pnas.0906817106

GENETICS

Correction for "Altered tumor formation and evolutionary selection of genetic variants in the human MDM4 oncogene," by Gurinder Singh Atwal, Tomas Kirchhoff, Elisabeth E. Bond, Marco Monagna, Chiara Menin, Roberta Bertorelle, Maria Chiara Scaini, Frank Bartel, Anja Böhnke, Christina Pempe, Elise Gradhand, Steffen Hauptmann, Kenneth Offit, Arnold J. Levine, and Gareth L. Bond, which appeared in issue 25, June 23, 2009, of *Proc Natl Acad Sci USA* (106:10236–10241; first published June 4, 2009; 10.1073/pnas.0901298106).

The authors note that the author name Marco Monagna should have appeared as Marco Montagna. The online version has been corrected. The corrected author line appears below.

Gurinder Singh Atwal, Tomas Kirchhoff, Elisabeth E. Bond, Marco Montagna, Chiara Menin, Roberta Bertorelle, Maria Chiara Scaini, Frank Bartel, Anja Böhnke, Christina Pempe, Elise Gradhand, Steffen Hauptmann, Kenneth Offit, Arnold J. Levine, and Gareth L. Bond

www.pnas.org/cgi/doi/10.1073/pnas.0907031106